Development of the Second-Generation Oscillating Surge Wave Energy Converter with Variable Geometry

Preprint

Michael Kelly
South Dakota School of Mines and Technology

Nathan Tom, Yi-Hsiang Yu, Robert Thresher
National Renewable Energy Laboratory

To be presented at the International Society of Offshore and Polar Engineers' International Ocean and Polar Engineering Conference
San Francisco, California
June 25–30, 2017

NREL is a national laboratory of the U.S. Department of Energy
Office of Energy Efficiency & Renewable Energy
Operated by the Alliance for Sustainable Energy, LLC

This report is available at no cost from the National Renewable Energy Laboratory (NREL) at www.nrel.gov/publications.

Conference Paper
NREL/CP-5000-67919
July 2017

Contract No. DE-AC36-08GO28308

NOTICE

This report is available at no cost from the National Renewable Energy Laboratory (NREL) at www.nrel.gov/publications.

Available electronically at SciTech Connect http:/www.osti.gov/scitech

Available for a processing fee to U.S. Department of Energy and its contractors, in paper, from:

U.S. Department of Energy
Office of Scientific and Technical Information
P.O. Box 62
Oak Ridge, TN 37831-0062
OSTI http://www.osti.gov
Phone: 865.576.8401
Fax: 865.576.5728
Email: reports@osti.gov

Available for sale to the public, in paper, from:

U.S. Department of Commerce
National Technical Information Service
5301 Shawnee Road
Alexandria, VA 22312
NTIS http://www.ntis.gov
Phone: 800.553.6847 or 703.605.6000
Fax: 703.605.6900
Email: orders@ntis.gov

Cover Photos by Dennis Schroeder: (left to right) NREL 26173, NREL 18302, NREL 19758, NREL 29642, NREL 19795.

NREL prints on paper that contains recycled content.

Development of the Second-Generation Oscillating Surge Wave Energy Converter with Variable Geometry

Michael Kelly,[1] Nathan Tom,[2] Yi-Hsiang Yu,[2] Robert Thresher[2]

[1]South Dakota School of Mines and Technology
Rapid City, South Dakota, USA

[2]National Renewable Energy Laboratory
Golden, Colorado, USA

ABSTRACT

This study investigates the effect of design changes on the hydrodynamics of a novel oscillating surge wave energy converter being developed at the National Renewable Energy Laboratory. The design utilizes controllable geometry features to shed structural loads while maintaining a rated power over a greater number of sea states. The second-generation design will seek to provide a more refined control of performance because the first-generation design demonstrated performance reductions considered too large for smooth power output. Performance is evaluated using frequency domain analysis with consideration of a nonideal power-take-off system, with respect to power absorption, foundation loads, and power-take-off torque.

KEY WORDS: Hydrodynamics; wave energy; power take-off; variable geometry; control

INTRODUCTION

The field of wave energy conversion is at an exciting point in development where many different kinds of technologies are being investigated, but the cost of energy from these wave energy converters (WECs) is too high to compete with other sources of energy generation. For wave energy to become competitive, WECs will need to adapt their performance so that maximum power is absorbed for all normal sea states, and so that loads can be shed in extreme conditions to reduce the structural and material costs for converters (Musial et al., 2013).

Recent work at the National Renewable Energy Laboratory (NREL) is focused on lowering the cost of energy of these devices by developing an oscillating surge wave energy converter (OSWEC) with controllable geometry. The novel OSWEC design utilizes the controllable geometry features to shed structural loads while maintaining a rated power over a greater number of sea states. This approach was first demonstrated with the first-generation design (Gen 1) that consists of a body comprised of four equal-size horizontal flaps spanning the length of the converter, see Fig. 1. The flaps are allowed to rotate, thereby altering the converter geometry and its hydrodynamic properties. The Gen 1 design demonstrated the ability to adapt its performance using the controllable geometry, but changes to the hydrodynamic properties with each open flap were considered too large for smooth power production in greater sea states (Tom et al., 2016a, 2016b). The second-generation (Gen 2) design will seek to address these large jumps and allow for finer control of performance using smaller controllable geometry sections.

The development of nearshore OSWECs has so far been led by Aquamarine Power's Oyster (Whittaker and Foley, 2012), AW-Energy's WaveRoller (Lucas, 2012), and Resolute Marine Energy's Surge WEC (Ramudu, 2011), which all consist of rigid bodies without controllable geometry. An early attempt to use controllable geometry in the form of airfoils arose with Atargis Energy Corporation's cycloidal device (Siegal, 2011). Additionally, Kurniawan and Moan (2012) investigated an OSWEC with a single controllable flap, for which the hydrodynamics were further tuned using ballast water to alter the rotational inertia. This device differs from the NREL converter because the NREL converter uses more control surfaces and power-take-off (PTO) control to tune the hydrodynamics for resonance.

This paper first reviews the Gen 1 design and introduces the changes made for the Gen 2 design. The hydrodynamics of the two designs are then compared to determine the effect of the geometric design changes. Along with the horizontal-flap-axis designs, the hydrodynamics of a vertical-flap-axis version of the Gen 2 design are investigated. Following the hydrodynamic modeling, a linear frequency domain analysis is used to evaluate both the horizontal and vertical Gen 2 designs for regular waves. Device performance is evaluated with respect to power absorption, foundation loads, peak-to-average power ratio, and PTO torque.

To make the analysis more realistic, constraints were set on the amplitude of pitch rotational motion. The geometry of the OSWEC is controlled on a sea-to-sea timescale, whereas the PTO is controlled on a wave-to-wave basis. Reactive PTO control is used to enact artificial resonance for the OSWEC at each frequency, which entails a bidirectional power flow that may return energy to the wave system during periods of the wave cycle. It is known that this bidirectional

flow causes inefficiencies when absorbing and transmitting power, so a nonideal PTO is considered for this analysis. Theoretical expressions to account for the effects of a nonideal PTO have been derived by Genest et al. (2014) and Falcao (2015). However, these papers looked at heaving WECs rather than pitching WECs. In this paper, the time-averaged power (TAP) sent to the grid is evaluated for the case where the PTO coefficients are chosen to optimize power absorption.

WAVE ENERGY CONVERTER DESCRIPTION

The wave energy converter can be thought of as a plate hinged at the ocean floor, restricted to rotate in the pitch angular direction. The base outer dimensions of the Gen 2 design, shown in Table 1, are mostly the same as those of the Gen 1 design. A conceptual rendering of the two OSWEC designs can be found in Figure 1, in which all of the flaps have been set in the open position. These flaps will be controlled in a binary fashion, in which actuators inside the WEC allow for only fully open or closed configurations. The structural mass is assumed to be evenly distributed, the structural mass density, ρ_m, was set to half of the fluid density, ρ_w, and the pitch moment of inertia, I_{55}, and hydrostatic restoring coefficient, C_{55}, are assumed to remain constant for each flap configuration.

The main difference in the Gen 2 design from the Gen 1 design comes from the size of the controllable geometry sections. The total area of the controllable geometry sections in Gen 2 is roughly a quarter of the Gen 1 section area. The other major change is in the number and size of the controllable flaps. Gen 1 has four equal-length elliptical

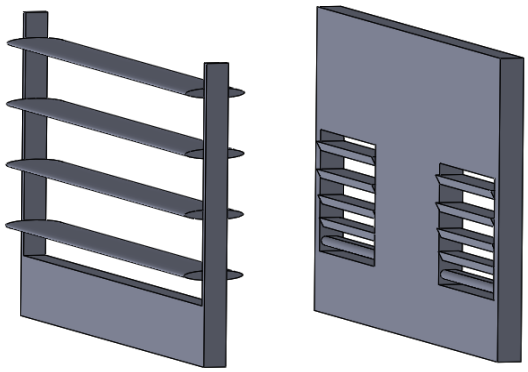

Fig. 1: First-generation (Gen 1) (left) and second-generation (Gen 2) (right) designs

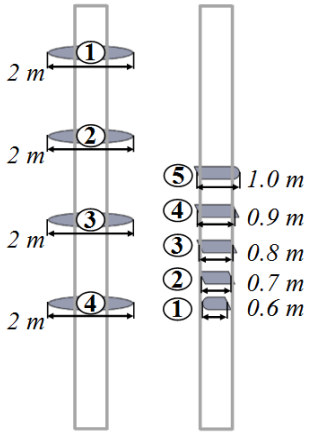

Fig. 2: Side view of the Gen 1 (left) and Gen 2 design (right) with flap dimensions and the order in which the flaps open for each design

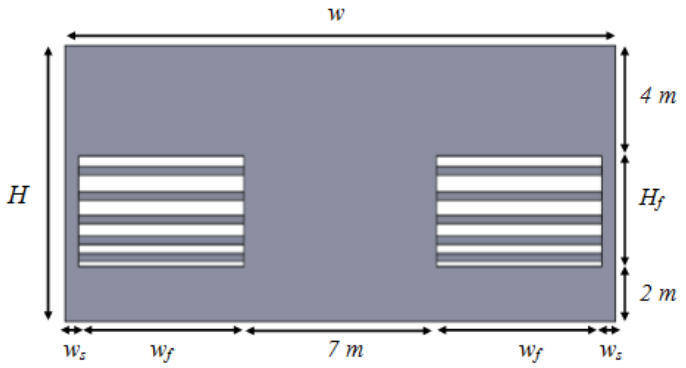

Fig. 3: Front view of the Gen 2 design with horizontal flaps

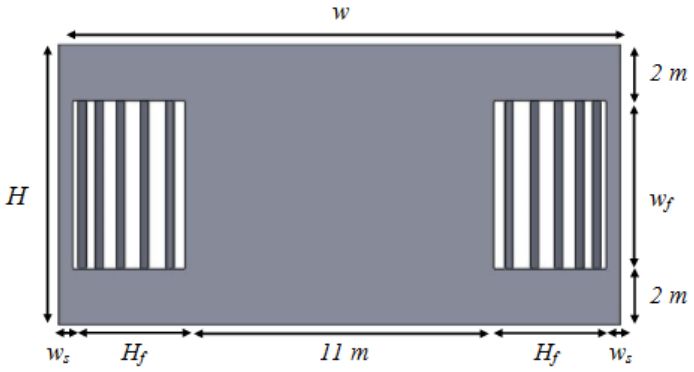

Fig. 4: Front view of the Gen 2 design with vertical flaps

Table 1. Geometric characteristics of the Gen 2 design

Water Depth	h	32.81 ft (10 m)	Flap Section Height	H_f	13.12 ft (4 m)
WEC Height	H	32.81 ft (10 m)	Flap Section Width	w_f	19.69 ft (6 m)
WEC Width	w	65.62 ft (20 m)	Flap Thickness	t_f	0.98 ft (0.3 m)
WEC Thickness	t	2.62 ft (0.8 m)	Center of Gravity	r_G	16.99 ft (5.18 m)
Support Width	w_s	1.64 ft (0.50 m)	Moment of Inertia	I_{55}	58424147 lb.ft^2 (2462 t.m^2)
Volume	V	4802.8 ft^3 (136 m^3)	Mass	m	74.96 US ton (68 t)

flaps that were opened from the top to bottom whereas Gen 2 has two sections of five flaps of varying lengths that are opened from bottom to top. Flaps one through five have lengths between 0.6 m and 1.0 m (see Figure 3), with each flap increasing by 0.1 m. The Gen 2 flaps are also shaped like parallelograms rather than ellipses, causing an interlocking pattern that mimics a flat plate when the flaps are closed. The parallelogram shape still allows for a somewhat streamlined shape when the flaps are open to try and reduce viscous losses, which was the goal of the elliptical flap shape in Gen 1.

This paper also analyzes a vertical variation in the Gen 2 design, wherein the controllable geometry flap axis is set to be vertical rather than horizontal. These flaps are the same size as the Gen 2 horizontal design, but are just reoriented, opening from the outside-in. The Gen 2 horizontal and vertical designs are shown in Figures 2 and 4, respectively.

HYDRODYNAMIC MODELING

Three-dimensional hydrodynamic modeling for all three WEC variations was conducted to see how the geometry design changes affect the converters' characteristics. Effect of device width and thickness on the hydrodynamics of the NREL WEC was previously investigated (Tom et al, 2016b). The hydrodynamic coefficients were obtained from WAMIT version 7.2 at a frequency step size of 0.01 rad/s for wave frequencies between 0.3 rad/s and 1.5 rad/s, or periods between 20.94 s and 4.19 s, respectively. The hydrodynamic coefficients are shown in Fig. 5 and 6 for the Gen 1 (left column) and Gen 2 horizontal (middle column) configurations. Figure 5 corresponds to the radiation pitch added moment of inertia, μ_{55}, and pitch wave damping, λ_{55}, and Fig. 6 corresponds to the pitch wave-excitation torque magnitude, $|X_5|$, and phase, ϕ_5. In the right column of these two figures, the percent of the closed flaps value for the added moment of inertia and pitch excitation magnitude is compared for the Gen 2 horizontal and vertical configurations.

The coefficients are plotted for the variation in the number of open flaps for each design. Note that the Gen 1 design opens flaps by starting from the top and going down, whereas the Gen 2 horizontal design opens flaps from the bottom to the top (see Fig. 2). It can be observed that as the number of open flaps increases, the pitch radiation wave damping and pitch excitation moment decrease over the frequency spectrum, along with the pitch-added moment of inertia in the low-frequency range. In the high-frequency range, the trend reverses for the pitch-added moment of inertia and increases with the number of open flaps. As mentioned earlier, the Gen 1 demonstrates a large reduction (>50%) in the hydrodynamics as each flap is opened. This magnitude of reduction would be beneficial for a survival case in extreme storm conditions, but is not conducive to producing rated power over a large array of sea states. The Gen 2 horizontal design shows that it can indeed provide a more refined control of hydrodynamics with the opening of each additional flap.

The hydrodynamics of the Gen 2 vertical design were also modeled and found to be similar to the results for the Gen 2 horizontal design, with slight differences in the magnitude of the coefficients. The Gen 2 horizontal and vertical configurations are compared in the right columns of Fig. 5 and 6. Fig. 6c shows how the pitch excitation moment of each open flap configuration compares to the closed flaps configuration. It can be observed in the low-frequency range that the vertical configuration (solid lines) shows an almost linear reduction of ~10% with the opening of each additional flap, whereas the reduction for the horizontal configuration with one open flap is ~17% and then levels out to a ~9% reduction with each open flap after that. The excitation moment appears to converge towards the closed flaps value in the high-frequency range as the wavelength and period get smaller. In this frequency range, the dynamic wave pressure will not penetrate to the depth of the flaps. It can also be observed that in the low-frequency range the vertical design has a larger pitch excitation magnitude, but in the high-frequency range the horizontal design has higher excitation magnitudes. This outcome is caused by the fact that as the period and wavelength decrease, the dynamic pressure becomes isolated near the water's surface. The open dimension of the vertical design is closer to the surface than the horizontal design, so more of the pressure towards the top is balanced by flow through the flaps rather than being absorbed by the device.

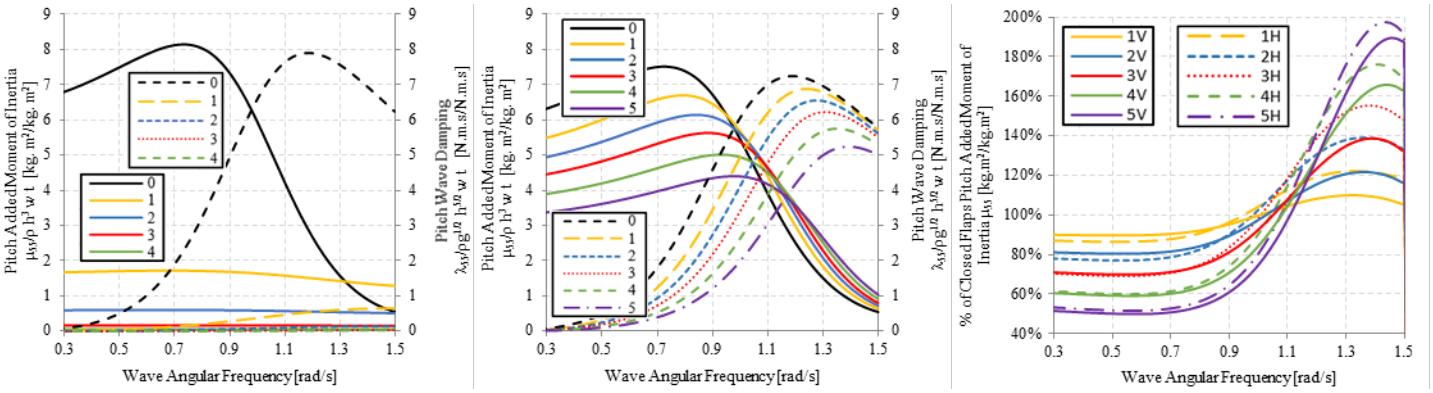

(a) Gen 1 horizontal (b) Gen 2 horizontal (c) Gen 2 horizonatal vs. Gen 2 vertical

Fig. 5: Variation in pitch-added mass, μ_{55}, and wave damping, λ_{55}, with the number of open flaps for the Gen 1 (a), Gen 2 horizontal (b) configurations, and the Gen 2 horizontal and vertical configurations (c). Solid lines correspond to the left axis and segmented lines correspond to the right axis for (a) and (b). In (c), solid lines represent the Gen 2 vertical results, and segmented lines represent the Gen 2 horizontal results.

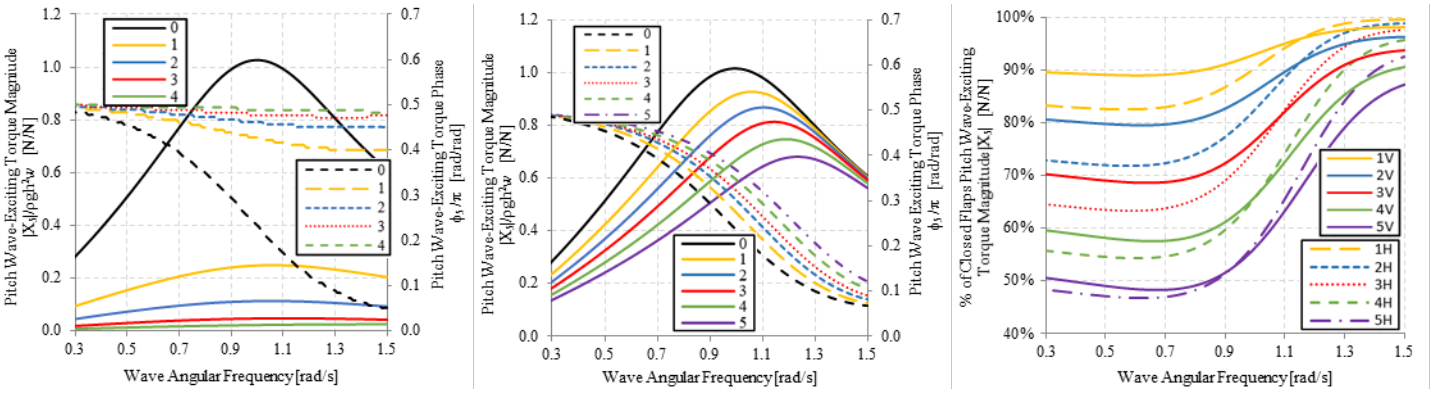

(a) Gen 1 horizontal (b) Gen 2 horizontal (c) Gen 2 horizontal vs. Gen 2 vertical

Fig. 6: Variation in pitch wave-excitation torque magnitude, $|X_5|$, and phase, ϕ_5, for each set of open flaps for the Gen 1 (a), and Gen 2 horizontal (b) configurations. Variation in pitch wave-excitation torque magnitude, $|X_5|$, for Gen 2 horizontal and vertical configurations (c), is also shown. Solid lines correspond to the left axis and segmented lines correspond to the right axis for (a) and (b). In (c), solid lines represent the Gen 2 vertical results, and segmented lines represent the Gen 2 horizontal results.

REGULAR WAVE ANALYSIS

This paper presents results from a frequency domain analysis that assumes linear wave theory. The fluid is assumed to be incompressible and inviscid, and have irrotational flow. The analysis considers the case of regular wave excitation with the incident wave elevation given as:

$$\eta(x,t) = \Re\left\{-\frac{1}{g}\frac{\partial \phi_0}{\partial t}\bigg|_{z=h}\right\} = A\cos(\sigma t - kx) \tag{1}$$

where ϕ_0 is the incident wave potential, A is the wave amplitude, σ is the wave angular frequency, and k is the wave number. The time harmonic response of the converter in the pitch degree of freedom is described by:

$$\zeta_5(t), \dot{\zeta}_5(t), \ddot{\zeta}_5(t) = \Re\{\xi_5 e^{i\sigma t}\}, \Re\{i\sigma\xi_5 e^{i\sigma t}\}, \Re\{-\sigma^2\xi_5 e^{i\sigma t}\} \tag{2}$$

where ζ_5, ζ_5*, and ζ_5** are the pitch angular displacement, velocity, and acceleration, and ξ_5 is the complex amplitude of pitch angular displacement. The one-degree-of-freedom time-domain pitch equation of motion is given as:

$$I_{55}\ddot{\zeta}_5(t) = \tau_h + \tau_e + \tau_r + \tau_{PTO} \tag{3}$$

where I_{55} is the pitch mass moment of inertia, τ_h is the hydrostatic restoring torque, τ_e is the wave-excitation torque, τ_r is the wave radiation, and τ_{PTO} is the mechanical torque applied by the PTO system. The hydrostatic restoring torque is described by:

$$\tau_h = \underbrace{(\rho V r_b - m r_g)g}_{C_{55}} \sin(\zeta_5(t)) \tag{4}$$

where ρ is the fluid density, V is the displaced volume, r_b is the center of buoyancy, m is the mass of the converter, and C_{55} is the hydrostatic pitch restoring coefficient for the OSWEC. The hydrostatic torque can be linearized by assuming a small pitch rotation where $\sin\zeta_5(t) \approx \zeta_5(t)$.

The wave excitation torque is given by:

$$\tau_e = \Re\{AX_5(\sigma)e^{i\sigma t}\} \tag{5}$$

The wave radiation torque is given by:

$$\tau_r = -\Re\{(-\sigma^2\mu_{55}(\sigma) + i\sigma\lambda_{55}(\sigma))\xi_5 e^{i\sigma t}\} \tag{6}$$

where μ_{55} is the pitch radiation added moment of inertia and λ_{55} is the pitch wave damping.

The mechanical torque applied by the PTO is described by:

$$\tau_{PTO} = -\Re\{(C_g + i\sigma\lambda_g)\xi_5 e^{i\sigma t}\} \tag{7}$$

where C_g is the PTO restoring coefficient and λ_g is the PTO damping coefficient. The selection of values for C_g and λ_g will be described later in this section.

After substituting the frequency domain expressions for the torques in Eq. 3 and rearranging, the frequency domain equation of motion is given by:

$$\xi_5(-\sigma^2(I_{55}+\mu_{55}) + i\sigma(\lambda_{55}+\lambda_g) + (C_{55}+C_g)) = AX_5 \tag{8}$$

The pitch angular displacement response amplitude operator (RAO) can be found from Eq. 8 and is shown in Eq. 9. The RAO allows many other performance values of the WEC to be calculated.

$$\frac{\xi_5}{A} = \frac{X_5}{[C_{55}+C_g-\sigma^2(I_{55}+\mu_{55})] + i\sigma[\lambda_{55}+\lambda_g]} \tag{9}$$

The PTO-absorbed TAP per wave amplitude squared by an ideal PTO can be found by integrating the instantaneous absorbed power over the wave period, which results in:

$$\frac{P_T}{A^2} = \frac{1}{2}\lambda_g \sigma^2 \left|\frac{\xi_5}{A}\right|^2 \tag{10}$$

The maximum PTO-absorbed TAP, per wave amplitude squared, for a given wave frequency occurs when the device operates at resonance, which satisfies the optimum phase condition.

$$\left.\frac{P_T}{A^2}\right|_{\max} = \frac{1}{8}\frac{|X_5|^2}{\lambda_{55}} \tag{11}$$

The optimum amplitude condition is met when the PTO damping matches the wave radiation damping (Evans, 1976).

$$\lambda_g = \lambda_{55}\sqrt{1+\left(\frac{C_{55}+C_g-\sigma^2(I_{55}+\mu_{55})}{\sigma\lambda_{55}}\right)^2} \tag{12}$$

The TAP contained within a propagating wave, per meter crest width, is of interest because it gives a reference measure to evaluate the capture efficiency of the WEC, and is given by:

$$P_W = \frac{1}{2}\rho g A^2 \sqrt{\frac{g}{k}\tanh(kh)}\left(1+\frac{2kh}{\sinh(2kh)}\right) \tag{13}$$

where h is the water depth. The nondimensional capture width of the WEC, defined as the ratio of the PTO to wave TAP, is calculated from:

$$C_W = \frac{P_T}{wP_W} \tag{14}$$

where w is the converter width.

Reactive Control

It is commonly known that an oscillating OSWEC absorbs the most energy when operating at its resonant frequency. In an effort to absorb the maximum amount of power, the WECs in this paper all use reactive PTO control to simulate resonance at any wave frequency. This simulation is physically realized with an actuator that can handle bidirectional power flow. The actuator can absorb power from WEC motion caused by waves and also expend power by motoring the WEC into motion that matches the resonance frequency. To simulate the device in resonance at each wave frequency, the PTO restoring coefficient C_g is adjusted so that the hydrostatic restoring, pitch mass moment of inertia, and pitch-added moment of inertia coefficients are cancelled out:

$$C_g = -[C_{55} - \sigma^2(I_{55}+\mu_{55})] \tag{15}$$

This artificial resonance condition is the basis for complex-conjugate control (Falnes, 2002). For passive control, the PTO is prevented from returning energy to the wave system, which is met by setting $C_g = 0$.

Pitch Motion Constraints

In order for the WEC to simulate resonance, there are certain wave frequencies wherein the magnitude of pitch angular displacement is unrealistic and too large for linear theory. To compensate for this, constraints on pitch motion were set at $|\xi_5|_{max} = 30°$ ($\pi/6$ radians), which could physically be realized by end stops. The maximum TAP absorbed by the PTO changes after the introduction of motion constraints, as shown in Evans (1981). The expression is given as:

$$\frac{P_T}{A^2} = \frac{1}{8}\frac{|X_5|^2}{\lambda_{55}}[1 - H(1-\delta)(1-\delta)^2] \tag{16}$$

where $H(x)$ is the Heaviside step function and δ is the ratio of the constrained-to-optimal pitch angular velocity shown by:

$$\delta = \frac{2\sigma|\xi_5|_{\max}\lambda_{55}}{A|X_5|} \tag{17}$$

For passive control, when the magnitude of pitch motion becomes larger than the constraint, the following PTO damping coefficient is used to simulate the end stops:

$$\lambda_g = \sqrt{\left(\frac{A|X_5|}{\sigma|\xi_5|_{\max}}\right)^2 - \left[\frac{C_{55}+C_g}{\sigma} - \sigma\left(I_{55}+\mu_{55}\right)\right]^2} - \lambda_{55} \tag{18}$$

When the magnitude of pitch motion is within the constraint, the PTO damping coefficient from Eq. 12 is used for passive control. For reactive control, wherein artificial resonance is satisfied, the PTO damping coefficient required to meet the motion constraints is provided by:

$$\lambda_g = \lambda_{55}\left[1+\frac{2(1-\delta)}{\delta}H(1-\delta)\right] = \begin{cases} \lambda_{55} & , \ \delta > 1 \\ \dfrac{A|X_5|}{\sigma|\xi_5|_{\max}} - \lambda_{55} & , \ \delta < 1 \end{cases} \tag{19}$$

Nonideal Power-Take-Off Unit

Thus far, the analysis has assumed that the PTO system is ideal and has no energy losses. It has been shown that the bidirectional flow of power associated with reactive PTO control has a negative impact on the amount of power sent to the grid when considering a nonideal PTO with efficiencies less than unity (Genest et al., 2014). To account for the negative impact on power sent to the grid, we added in the consideration of a nonideal PTO for the TAP sent to the grid, which was previously derived (Strager et al., 2014; Falcao and Henriques, 2015) and given as:

$$P_O = \eta_e \frac{\lambda_g |i\sigma\xi_5|^2}{2}\left\{1+\frac{1-\eta_e^2}{\eta_e^2}\left[\frac{2G^* - \sin(2G^*) - 2G(1-\cos^2(G^*))}{2\pi}\right]\right\} \tag{20}$$

$$G = \left| \frac{C_g}{\sigma \lambda_g} \right| \tag{21}$$

$$G^* = \arctan(G) \tag{22}$$

where η_e is the PTO efficiency and G is the ratio of PTO reactance to resistance. Also under consideration with the nonideal PTO is the peak-to-average power ratio, which can have effects on the necessary PTO power capacity. This relation is given by:

$$PA_+ = \frac{1+\sqrt{1+G^2}}{1+\frac{1-\eta_e^{\,2}}{\eta_e^{\,2}}\left[\frac{2G^* - \sin(2G^*) - 2G(1-\cos^2(G^*))}{2\pi}\right]} \tag{23}$$

$$PA_- = \frac{1-\sqrt{1+G^2}}{\eta_e^{\,2}\left\{1+\frac{1-\eta_e^{\,2}}{\eta_e^{\,2}}\left[\frac{2G^* - \sin(2G^*) - 2G(1-\cos^2(G^*))}{2\pi}\right]\right\}} \tag{24}$$

Foundation Reaction Forces

In order for the WEC to stay stationary on the seabed, the foundation needs to withstand the reaction forces in the surge and heave directions, which are defined per-unit wave amplitude as X_{r1} and $X_{r3,}$ respectively. The equations for X_{r1} and X_{r3} were used by Kurniawan and Moan (2012) and are given as:

$$X_{r1} = \left[-\sigma^2 \mu_{15} + i\sigma\lambda_{15}\right]\frac{\xi_5}{A} - X_1 \tag{25}$$

$$X_{r3} \approx -X_3 \tag{26}$$

where X_1 and X_3 are the complex surge and heave wave-excitation forces per-unit wave amplitude, and μ_{15} and λ_{15} are the surge pitch-added mass and wave damping. An equation for the combination of the surge and heave reaction forces gives the maximum reaction force felt by the foundation (Kurniawan and Moan, 2013), which is given by:

$$X_r = \sqrt{\frac{1}{2}\left(\left|X_{r1}^2 + X_{r3}^2\right| + \left|X_{r1}\right|^2 + \left|X_{r3}\right|^2\right)} \tag{27}$$

REGULAR WAVE RESULTS

Performance characteristics for the Gen 2 horizontal and vertical configurations were evaluated with a linear frequency domain analysis for the case of regular waves. A wave amplitude of 1 m was considered, along with a pitch angular displacement constraint of $|\xi_5|_{max}$= 30° (π/6 radians) and a nonideal PTO system with an efficiency of 85%. The evaluated performance characteristics were the foundation reaction forces, PTO torque, peak-to-average power ratio, and TAP sent to the grid. The values were plotted for various flap configurations to show how performance changes with each additional flap opening (see Fig. 7, 8, and 9). As a reminder, the Gen 2 horizontal design opens flaps in order from the bottom to the top, whereas the Gen 2 vertical design opens flaps in order from the outside to the inside.

Some of the trends from the hydrodynamic modeling affected the performance characteristics, with reductions in magnitude as the number of open flaps increased. The plots of the vertical and horizontal configurations were nearly identical, so instead of having two similar figures, the characteristics are plotted for only the horizontal configuration. The horizontal and vertical configurations are compared as a percentage of the closed flaps performance value so that the differences between the two configurations can be more easily observed. The closed flaps performance values were equal for both the horizontal and vertical configurations because they are both a flat plate. It can be observed that as the number of open flaps increases, the maximum foundation reaction force, PTO torque, and TAP sent to the grid all decrease in a fairly linear fashion. This outcome highlights the success of the geometry design changes made for the Gen 2 device.

The peak-to-average power ratio (+ and -) increases in magnitude with the opening of each flap, as shown in Fig. 7(c). This ratio was calculated with consideration of a nonideal PTO, which produces larger magnitudes than for an ideal PTO. The peak-to-average power ratio is of interest because the higher the ratio, the larger the necessary PTO power capacity, which can have a direct impact on the cost of energy.

The Gen 2 horizontal and vertical designs are compared with respect to the foundation loads, PTO torque, and power-to-load ratio in Fig. 8. As observed, the vertical configuration experiences higher foundation loads over the whole frequency spectrum, whereas the horizontal configuration exposes the PTO to larger torque magnitudes for the majority of wave frequencies. These two performance characteristics are important because the foundation loads will affect the structural costs of the OSWEC, and large PTO torque magnitudes increase the fatigue damage on the PTO system.

The power-to-load ratio considered in Fig. 8(c) is defined by:

$$P_{tL} = \frac{P_T / A^2}{X_r + \tau_{PTO} / A} \tag{28}$$

which is one way to measure the success of the variable geometry concept. It considers the power sent to the grid as well as the foundation loads and torques on the PTO system. It can be observed that the P_{tL} ratio increases with the number of open flaps, meaning the reductions in power absorption are smaller than the reductions in foundation forces and PTO torque. The Gen 2 vertical design shows a larger power-to-load ratio over the majority of the spectrum than the horizontal configuration.

Consideration of a nonideal PTO at η_e=85% efficiency also allows for a more realistic understanding of the converter performance. The effect of PTO efficiency on TAP sent to the grid can be seen in Fig. 9(a), wherein the nonideal PTO produces ~85% of the output power of an ideal PTO for most of the wave spectrum, and less than that around 0.7 rad/s. Then Gen 2 horizontal and vertical designs are also compared with TAP sent to the grid compared to the closed flaps value in Fig. 9(b). It is shown that the vertical configuration produces more power in the low-frequency range and the horizontal configuration produces more power in the high-frequency range.

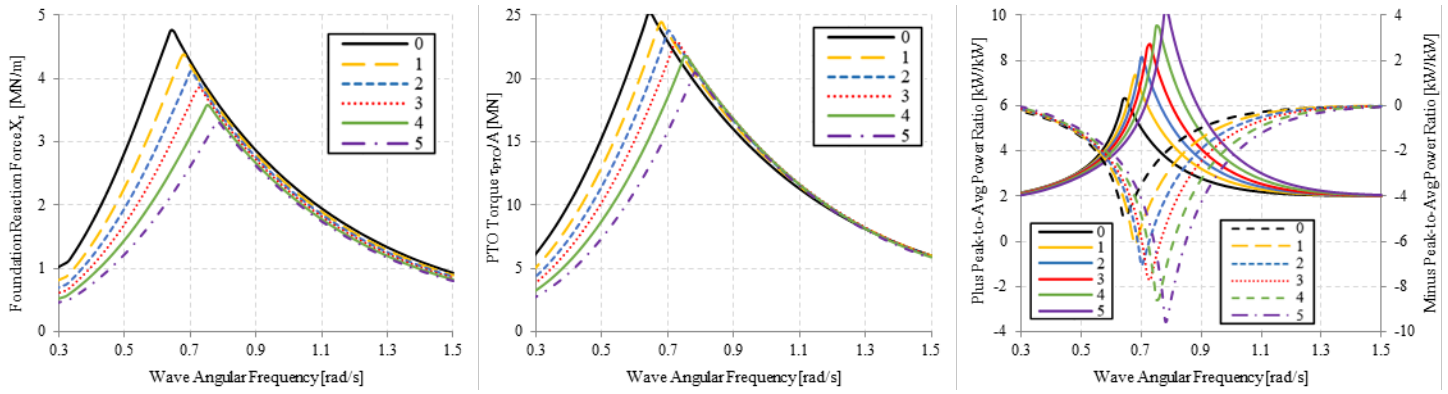

(a) Gen 2 horizontal foundation reaction forces (b) Gen 2 horizontal PTO torque (c) Gen 2 horizontal peak-to-avg TAP ratio (+ and -)

Fig. 7: Variation in foundation reaction forces, X_r (a), PTO torque, τ_{PTO}(b), and peak-to-average TAP ratio, P_a+ and P_a- (c) for the number of open flaps for the Gen 2 horizontal configuration. Solid lines in (c) correspond to the left axis and vice versa for segmented lines.

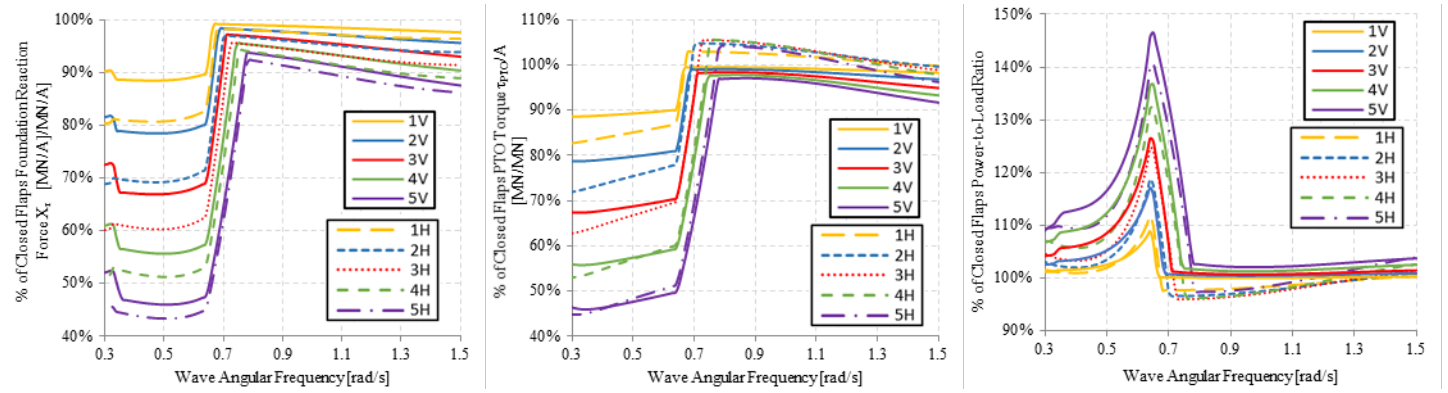

(a) Gen 2 horizontal (dotted) vs. Gen 2 vertical (solid) (b) Gen 2 horizontal (dotted) vs. Gen 2 vertical (solid) (c) Gen 2 horizontal (dotted) vs. Gen 2 vertical (solid)

Fig. 8: Variation in percent of closed flaps foundation reaction forces (a), PTO torque (b), and variation of the power-to-load ratio $[P_T/A^2 / (X_r + \tau_{PTO}/A)]$, with open flap number (c).

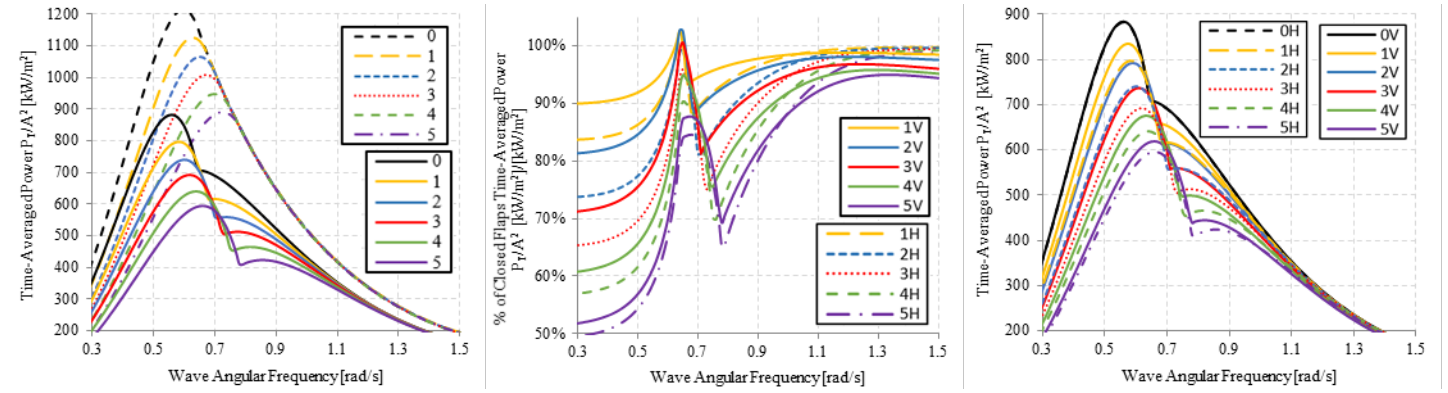

(a) Gen 2 horizontal η_e=85% vs. ideal PTO (b) Gen 2 horizontal vs. Gen 2 vertical (c) Gen 2 horizontal vs. Gen 2 vertical η_e=85%

Fig. 9: Variation in TAP sent to the grid, P_T/A^2, for the Gen 2 horizontal design with an ideal PTO and 85%-efficient PTO (a), the percentage of closed flaps TAP sent to the grid with a 85% PTO efficiency (b), and a comparison of the Gen 2 horizontal and vertical TAP sent to the grid with a PTO efficiency of 85% (c).

CONCLUSIONS

This paper investigates the effects of geometry changes on the performance of the novel OSWEC with control surfaces that has been under development at NREL. It was shown that the second-generation design provided for a more refined control of the hydrodynamic properties of the OSWEC, and that having the flaps oriented horizontally or vertically had little effect on the hydrodynamic coefficients for this design. The vertical configuration provided a more linear reduction with the opening of each flap, but the shape of the vertical and horizontal plots matched very closely.

A frequency domain analysis was carried out for the second-generation horizontal and vertical configurations to determine the performance of the new design. Performance characteristics of interest were the TAP sent to the grid, PTO torque, maximum foundation reaction forces, and peak-to-average power ratio. Reactive control of the PTO with a bidirectional power flow was used to enact artificial resonance on the WEC, so a nonideal PTO with an efficiency of 85% was considered. Constraints were set on pitch angular motion to simulate end stops, because the optimal amplitude of motion for artificial resonance can sometimes have unrealistic values. It was observed that the orientation of the flaps also had little effect on the performance characteristics, with only small variations in value between the horizontal and vertical configurations. The vertical configuration did allow for a more linear reduction in performance characteristics and a larger power-to-load ratio, so additional analysis will need to be done to select the final orientation for the OSWEC.

This preliminary analysis has shown that the second-generation design is a better fit for adjusting its performance to generate a rated power over a wider array of wave conditions than the first generation, while still allowing for a reduction in foundational and PTO loads.

ACKNOWLEDGEMENTS

This work was supported by the U.S. Department of Energy under Contract No. DE-AC36-08GO28308 with the National Renewable Energy Laboratory. Funding for the work was provided by NREL's Laboratory Directed Research and Development Program. The U.S. Government retains and the publisher, by accepting the article for publication, acknowledges that the U.S. Government retains a nonexclusive, paid-up, irrevocable, worldwide license to publish or reproduce the published form of this work, or allow others to do so, for U.S. Government purposes.

REFERENCES

Falcao, A, and Henriques, J (2015). "Effect of non-ideal power take-off efficiency on performance of single- and two-body reactively controlled wave energy converters. *Journal of Ocean Engineering and Marine Energy*, 1 (3), 273-286.

Evans, D V (1976). "A theory for wave-power absorption by oscillating bodies." *Journal of Fluid Mechanics*, 77(1), 1-25.

Evans, D V (1981). "Maximum wave-power absorption under motion constraints. *Applied Ocean Research*, 3(4), 200-203.

Genest, R, Bonnefoy, F, Clément, AH, and Babarit, A (2014). "Effect of non-ideal power take-off on the energy absorption of a reactively controlled one degree of freedom wave energy converter." *Applied Ocean Research*, 48, 236-243.

Kurniawan, A, and Moan, T (2012). "Characteristics of a pitching wave absorber with rotatable flap." *Energy Procedia 2012*, 20, 134-147.

Kurniawan, A, and Moan, T (2013). "Optimal geometries for wave absorbers oscillated about a fixed axis." *IEEE Journal of Ocean Engineering*, 38(1), 117-130.

Lucas, J, Livingstone, M, Vuorinen, M, and Cruz, J (2012). "Development of a wave energy converter (WEC) design tool – application to the WaveRoller." *Fourth International Conference on Ocean Energy,* Dublin, Ireland.

Musial, W, Lawson, M, and Rooney, S (2013). Marine Hydrokinetic technology (MHK) instrumentation, measurement, and computer modeling workshop. National Renewable Energy Laboratory, Technical Report. NREL/TP-5000-57605.

Ramudu, E (2011). "Ocean wave energy-driven desalination systems for off-grid communities in developing countries." *Proc of the IEEE Global Humanitarian Technology Conference*, 1129-1142.

Siegel, SG, Fagley, C, Romer, M, and McLaughlin, TE (2011). "Experimental wave cancellation using a cycloidal wave energy converter." *Proc Of the 9th European wave and tidal energy conference*.

Strager, T, Martin dit Neuville, A, Fernández López, P, Giorgio, G, Mureşan, T, Andersen, P, Nielsen, KM, Pedersen, TS, and Vidal Sánchez, E (2014). "Optimising reactive control in non-ideal efficiency wave energy converters." *Proc of the 33rd International Conference on Ocean, Offshore, and Arctic Engineering (OMAE2014),* San Francisco, USA.

Tom, N, Lawson, M, Yu, Y-H, and Wright, A (2015). "Preliminary analysis of an oscillating surge wave energy converter with controlled geometry." *Proc. Of the 11th European wave and tidal energy conference*.

Tom, N, Lawson, M, Yu, Y-H, and Wright, A (2016a). "Spectral modeling of an oscillating surge wave energy converter with control surfaces." *Applied Ocean Research*, 56, 143-156.

Tom, N, Lawson, M, Yu, Y-H, and Wright, A (2016b). "Development of a nearshore oscillating surge wave energy converter with variable geometry." *Renewable Energy*, 96, 410-424.

Whittaker, T, and Folley, M (2012). "Nearshore oscillating wave surge converters and the development of Oyster. *Philosophical Transactions Royal Society A,* 370, 345-364.